

Article

Synoptic-Scale Wildland Fire Weather Conditions in Mexico

Hiroshi Hayasaka 

Arctic Research Center, Hokkaido University, Sapporo 0010021, Japan; hhaya@eng.hokudai.ac.jp;
Tel.: +81-11-706-9074

Abstract: Future climate change is expected to increase the risk and severity of wildland fires in tropical regions. Synoptic-scale fire weather conditions in Mexico were carefully analyzed using 20 years of satellite hotspot and rainfall data, hourly weather data, and various climate data. Fire analysis results showed that eighty-four percent of all fires in Mexico occurred south of 22° N. Southwest Mexico (SWM, N < 22°, 94–106° W) and Southeast Mexico (SEM, N < 22°, 86–94° W), account for 50% and 34% of all fires in Mexico. Synoptic-scale analysis results using hourly data showed that westerly wind sea breezes from the Pacific Ocean blow toward the coastal land areas of the SWM while easterly wind sea breezes from the Caribbean blow into the SEM. The most sensitive weather parameters were “relative humidity” for the SWM and “temperature” for the SEM. The fire-related indices selected were “precipitable water vapor anomaly” for the SWM and “temperature anomaly” for the SEM. The SWM fire index suggests that future fires will depend on dryness, while the SEM fire index suggests that future fires will depend on temperature trends. I do hope that this paper will improve local fire forecasts and help analyze future fire trends under global warming in Mexico.

Keywords: wildland fire; synoptic meteorology; climate change; satellite hotspot; precipitable water vapor; air temperature; Mexico



Citation: Hayasaka, H. Synoptic-Scale Wildland Fire Weather Conditions in Mexico. *Atmosphere* **2024**, *15*, 96. <https://doi.org/10.3390/atmos15010096>

Academic Editor: Chuixiang Yi

Received: 16 December 2023

Revised: 7 January 2024

Accepted: 9 January 2024

Published: 11 January 2024



Copyright: © 2024 by the author. Licensee MDPI, Basel, Switzerland. This article is an open access article distributed under the terms and conditions of the Creative Commons Attribution (CC BY) license (<https://creativecommons.org/licenses/by/4.0/>).

1. Introduction

Across Earth’s ecosystems, wildland fires are growing in intensity and spreading in range. Wildland fires are wreaking havoc on the environment, wildlife, human health, and infrastructure [1]. Global annual burnt area is currently estimated to be between 4.2 and 4.7 million km² [2–4]. The tropics experience more fires than anywhere else on Earth. [5]. Residing between the Tropics of Cancer and Capricorn, the tropics are comprised of everything from the lushest of rainforests to the harshest of deserts. They cover one-third (33.7%) of the land surface of the planet, contain over 40% of all forests, over 35% of all people, and the vast majority of all species [6]. In recent decades, the largest fires have occurred in tropical ecosystems, burning millions of hectares [7], causing billions of dollars in economic damages, and impacting the health of millions of people in several countries [8].

Indonesia has one of the highest rates of deforestation and forest degradation in the world. The main causes are agricultural expansion and timber extraction, as well as increasing incidence of forest fires [9–12]. Indonesian peatlands store an estimated 57 Gt of carbon, 55% of the world’s tropical peatland carbon [13,14]. Indonesia’s peatlands have been extensively degraded and peatland fires are on the rise, especially in Central Kalimantan (Borneo), where large-scale agricultural land development has taken place and peatland fires occur annually [15]. The largest development is Mega Rice Project (MRP). Recurring peatland fires throughout Central Kalimantan have resulted in severe economic and social impacts for local people, along with globally significant environmental impacts.

Amazon forests contain nearly half of the world’s tropical forest carbon stocks [8]. Although natural fires are extremely rare in the Amazon, a combination of deforestation, changing land-use practices, and droughts have made this ecosystem susceptible

to wildfire [16,17]. Over the past two decades, droughts and heatwaves have become more frequent and severe [18,19]. These hot and dry periods increase tree mortality and vulnerability to fire [20]. Deforestation fragments the forest, which also has an impact on the increase in fire incidence at the forest edges and patches. Ninety-five per cent of active fires, and the most intense fires, are found within 1 km of the forest edge [21].

In sub-Saharan Africa, the grassy savanna biomes dry out annually and provide the fuel for fires. African savannas and the variability and interactions between rainfall, humans, and fire, enable the turnover in grass biomass [22] and the coexistence of trees and grass cover [23,24]. In large parts of Africa, where there is less than 800 mm of rainfall annually, increased temperatures and droughts result in less burnt area due to a decline in grass biomass and productivity [25]. Therefore, not all ecosystems burn more when exposed to drought and high temperatures. In these arid regions of Africa, it is actually periods of increased rainfall that lead to higher fire activity due to greater accumulated biomass [26].

Climate change, along with human activity, is playing an increasingly large role in determining wildfire regimes, and future climate change is expected to increase the risk and severity of wildfires in many biomes, including tropical rainforests [27]. All fire-prone countries and regions of the world need to develop comprehensive fire management plans to predict the risk and severity of future wildfires. To this end, it is necessary to understand the current status of fires and to identify fire weather conditions and fire related indices.

The main research objective is to identify fire weather conditions in different regions of the world and understand how these weather conditions will affect fire regimes under climate change. To achieve this objective, I have already conducted synoptic weather analysis to explain wildland fires in boreal regions, such as Alaska and Siberia, and reported that fires became active under strong winds associated with either high- or low-pressure systems. There were various weather patterns and no common conditions. However, most fires were found to occur commonly under warm air masses such as the continental temperate (cTe) migrating from desert regions such as the Great Basin, located in the subtropical high-pressure belt (STHP, around 30–40° N) [28–31]. For fires in tropical regions between north and south STHP, it was difficult to apply synoptic weather analysis in the tropics because of the large diurnal variations in temperature that generate sea breezes. To evaluate diurnal temperature change and sea breeze, hourly data should be used, and I found hourly data on the web for regional airports in most countries, including Mexico (hourly weather data from weather underground (for example: Villahermosa in Mexico; <https://www.wunderground.com/history/daily/mx/centro/MMVA/date/2021-5-3> (accessed on 6 December 2023))). Using hourly data, I confirm the occurrence of sea breezes (air masses from the ocean) and understand their meteorological characteristics.

This paper introduces a unique fire analysis method using hourly data for local airports. This proposed method obtains all fire-related data necessary for analysis from the Internet, so anyone can conduct fire analysis in any country or specific region. The data we used were 20 years of fire data and hourly data on basic weather parameters such as temperature, humidity, wind direction and speed, and atmospheric pressure. Analysis using hourly weather data can more clearly show fire weather and sea breeze conditions, and fire-related indices in the tropics, where weather conditions have large diurnal ranges. This method extracts fire-prone weather conditions and has also been used to determine fire weather conditions and fire-related index on three Indonesian islands (Sumatra [32,33], Kalimantan (Borneo) [34], and Papua [35]).

The present paper describes how the analytical method is applied to Mexico. The analysis methods and procedures are shown in the flowchart diagram in Section 2 (Materials and Methods). The first part of Section 3 (Results) describes how to analyze and evaluate 20 years of fire data obtained from the Internet. Next, I describe how I analyzed hourly data such as temperature, humidity, wind direction and speed, and atmospheric pressure during active fire periods in fire-prone areas of Mexico. Section 4 (Discussion) describes the

fire indices selected based on the fire weather analysis results and their evaluation results. The conclusions are presented in Section 5.

2. Materials and Methods

2.1. Study Area

Figure 1 shows the study area. Mexico is located between latitudes 14° and 33° N and longitudes 86° and 119° W in the southern portion of North America. The total area is about $1,973,000$ km². The Great Divide is located primarily in the mountainous region of Mexico. Mexico has coastlines on the Pacific Ocean and Gulf of California, as well as the Gulf of Mexico and the Caribbean (the western part of the Atlantic Ocean). The California Current (cold current), the Pacific Equatorial Current (warm current), and the Caribbean Current (warm current), flow in each ocean. The flow of these ocean currents is roughly indicated by straight lines with arrows.

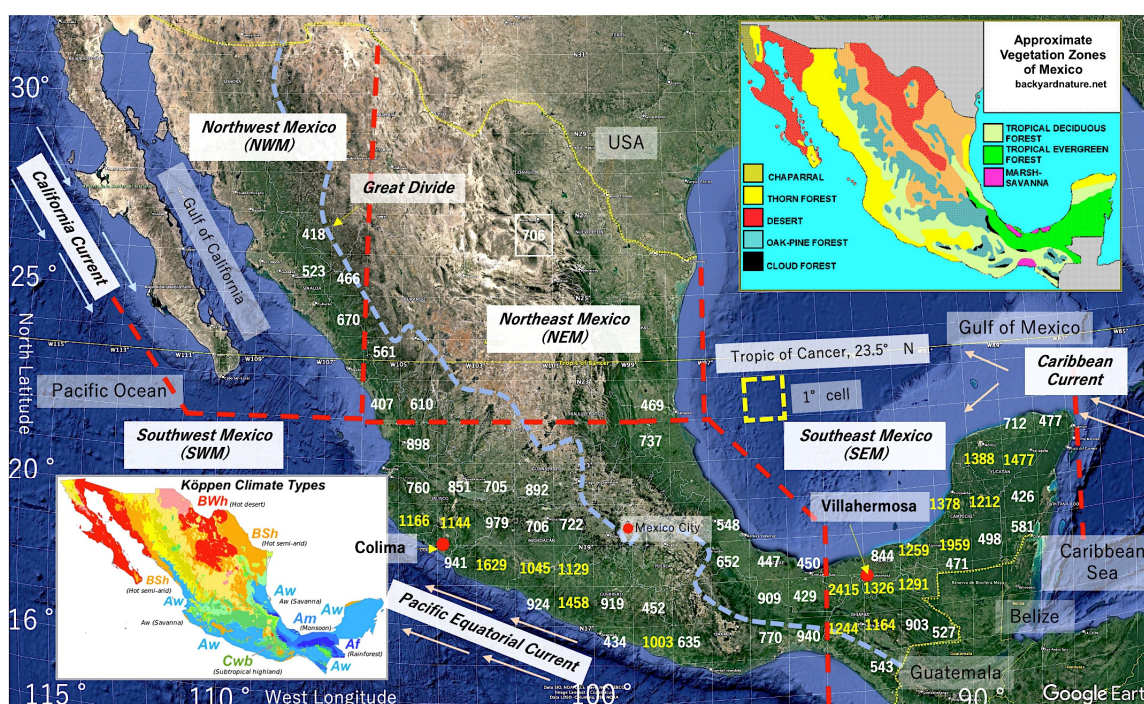


Figure 1. Map of the study area, Mexico ($14\text{--}33^{\circ}$ N, $86\text{--}119^{\circ}$ W). The vegetation zones in Mexico are shown in the upper right corner of the figure. The Köppen climate types in Mexico are shown in the lower left corner of the figure. The red dashed lines are the boundaries of the four areas that have been tentatively determined. The four areas are called Southeast Mexico (SEM), Southwest Mexico (SWM), Northeast Mexico (NEM), and Northwest Mexico (NWM). Fire distribution is shown by the number of satellite hotspots (HSs) for each 1° grid cell (the yellow dashed line rectangle shows its size at $25\text{--}26^{\circ}$ N in the Gulf of Mexico). All numbers such as 770, 1244 in each grid cell are the average number of hotspots (HSs year⁻¹) of the last 20 years, from 2003. Values for fire-prone grid cells (HSs > 1000) are shown in yellow, while values for weak fire grid cells (HSs < 400), are not shown. Total number of hotspots of 20 years from 2003 was 1,401,061. Three red circles, from left to right, indicate the locations of Colima, Mexico City (capital of Mexico), and Villahermosa. The blue dashed line indicates the approximate location of the Great Divide (The Great Continental Divide of the Americas, <https://commons.wikimedia.org/wiki/File:NorthAmerica-WaterDivides.png>, accessed on 6 January 2024). For the names of ocean currents and their directions, we referred to diagrams in the Encyclopedia Britannica. (<https://www.britannica.com/place/California-Current#/media/1/89578/46367>, accessed on 6 January 2024). Base Map: Google Earth Pro. Vegetation Map: backyardnature.net. Köppen Climate Region Map (https://en.wikipedia.org/wiki/Climate_of_Mexico#/media/File:Mexico_Köppen.svg, accessed on 6 December 2023)) are.

Wildland fire distributions in Mexico are analyzed using 1° grid cells (the yellow dashed line rectangle shows its size at 22–23° N in Figure 1), where I counted the number of satellite hotspots (HSs) of each 1° grid cell.

Based on the distribution of fire, vegetation, and climate, Mexico is divided into four regions for the sake of simplicity. Those four regions are called Southeast Mexico (SEM), Southwest Mexico (SWM), Northeast Mexico (NEM), and Northwest Mexico (NWM) in this paper. Their boundaries are shown by red dashed lines in Figure 1. Two local towns, Villahermosa and Colima, shown in Figure 1, are selected to discuss fire weather conditions in Mexico, as they are located in the most active fire areas in Mexico.

2.2. Analysis Methods and Procedures

Figure 2 shows analysis methods and procedures. All data required for analysis were obtained on the Internet in this paper. The analysis consists of four steps. First, satellite observation fire data was analyzed to assess the spatiotemporal distribution of fires in Mexico and identify fire-prone areas. In the second step, strongest and weakest active fire periods were extracted from very active and weak fire years, respectively. Then, fundamental weather conditions during fire periods were compared to extract fire-prone weather conditions using hourly data at weather stations in the third step. Lastly, fire-related indices were selected by comparing their coefficient of determination values to improve fire forecasts in each fire-prone area in Mexico, and to help analyze future fire trends under global warming.

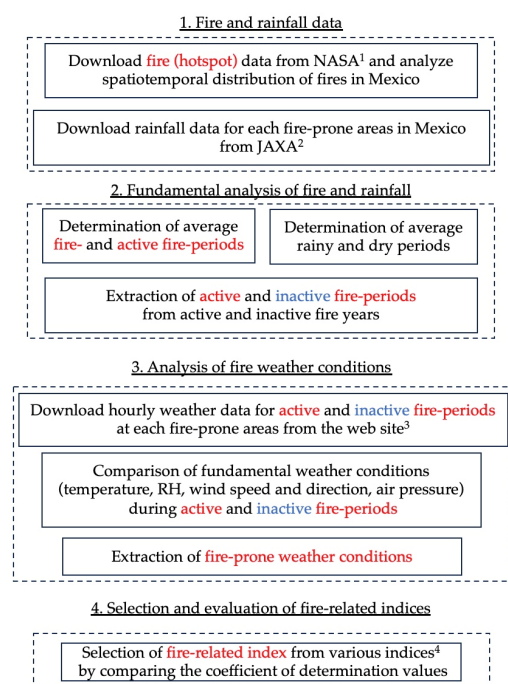


Figure 2. Analysis methods and procedures. ¹ NASA Fire Information for Resource Management System (MODIS Collection 6.1, <https://firms2.modaps.eosdis.nasa.gov/download/> (accessed on 15 May 2023) with a pixel resolution of 1 km. Total number of hotspots was 1,401,061. ² Rainfall data from the JAXA (https://sharaku.eorc.jaxa.jp/GSMaP_CLM/index.htm, accessed on 1 October 2023). ³ Hourly weather data from weather underground (Villahermosa: <https://www.wunderground.com/history/daily/mx/centro/MMVA/date/2021-5-3>, Colima: <https://www.wunderground.com/history/daily/mx/cuauhtemoc/MMIA/date/2020-5-16>, accessed on 11 August 2023). ⁴ NCEP/NCAR 40-year reanalysis data (<https://psl.noaa.gov/data/composites/day/>, accessed on 15 August 2023). Coverage and spatial resolution of the NCEP reanalysis data are geographic longitude and latitude: 0.0–358.125° E, –88.542° N to 88.542° N; spatial resolution: about 2.5° × 2.5°; period and temporal resolution: 1 January 1948 to now, 6-hourly, daily, and monthly.

2.2.1. Fire and Rainfall Data

Many researchers use NASA hotspot (HS) data to analyze fires around the world [1]. This paper also used NASA HS data as the fire database in Mexico. Daily hotspot (HS) data over 20 years from 1 January 2003 to 31 December 2022, detected by Moderate Resolution Imaging Spectroradiometer (MODIS) on the Terra and Aqua satellites, were obtained from the NASA Fire Information for Resource Management System (see more in the caption in Figure 2) and used to analyze the spatiotemporal distribution of fires in Mexico. Hotspot analysis results showed fire-prone areas in Mexico and the average active fire periods over the last 20 years.

For each fire-prone area in Mexico, satellite-derived rainfall data provided by Japan Aerospace Exploration Agency (JAXA) were downloaded from its web page (see caption for Figure 2). They are processing information from multiple precipitation-observing satellites and geostationary meteorological satellites. The average dry and wet seasons for each region of Mexico were determined using 20 years of rainfall data from 2003 to 2022.

Active fires, or the spatiotemporal distribution of fires, in Mexico and various weather conditions such as cloud distribution were also checked using the satellite imageries of Worldview [36]. Various weather conditions were also checked using the data from Villahermosa and Colima from Weather Spark [37].

2.2.2. Fundamental Analysis of Fire and Rainfall

Daily hotspot (HS) data were used to identify average fire and active fire periods, as well as yearly, monthly, weekly, and daily fire occurrence. Average fire and active fire periods were determined from trends of daily fire occurrence. To discuss fire weather conditions, two fire periods were selected from active and inactive fire years. Then, they were labeled as the most active and most inactive fire periods in this paper. The most active fire period was extracted from the period of the year with the largest annual HS number, and the most inactive fire period was extracted from the period of the year with the smallest annual HS number.

2.2.3. Analysis of Fire Weather Conditions

For the most active and inactive fire periods of each fire-prone area in Mexico, hourly fundamental weather data (temperature, relative humidity, wind speed and direction, air pressure, and weather types) was measured at the airport stations in Colima and Villahermosa and were obtained from the web site “Weather Underground” (see caption for Figure 2). The measurement local times at the two stations were random, such as 10:29 (=10.48) and 12:31 (=12.52), so these times were rounded to the nearest 10:00 and 13:00, respectively. These time corrections made it easier to plot fire weather data on a single graph.

From comparison of fundamental weather conditions during the most active and inactive fire periods, I could extract major fire-related weather conditions, such as temperature-dependence, RH-dependence, air pressure-dependence, and so on.

2.2.4. Selection of Fire-Related Indices

Fire-related indices, except Nino 3 and 4 and Pacific Decadal Oscillation (PDO), were mostly selected from various indices on the web site of NCEP/NCAR from the 40-year reanalysis data (see caption for Figure 2). Candidate indices are composites of various weather maps at the lower (1000, 925, and 850 hPa) and the middle (500 hPa), and their anomaly maps; temperature maps at 850 and 1000 hPa and these anomaly maps; precipitable water vapor (PWV); outgoing longwave radiation (OLR); Nino SST Index (Nino 3 and 4); Pacific Decadal Oscillation (PDO); sea surface temperature (SST) and its anomalies at near Mexico.

Two major climate indices, Nino SST Index (Nino 3 and 4) and Pacific Decadal Oscillation (PDO), were obtained from the following web sites: Nino 3 and 4, <https://www.cpc.ncep.noaa.gov/data/indices/sstoi.indices>, (accessed on 13 October 2023),

PDO, <https://www.ncei.noaa.gov/pub/data/cmb/ersst/v5/index/ersst.v5.pdo.dat>, (accessed on 13 October 2023). Worldview [36] was used for the preliminary check. They also provide various fire-related information such as haze, OLR, PWV, surface conditions, and cloud distribution.

3. Results

3.1. Fire (Hotspots) Distribution in Mexico

A total of 1,401,061 hotspots (HSs) were detected during the 20-year period from 2003 to 2022. To show HSs distribution in Mexico, the number of HSs in each 1° grid cell was used. Figures such as 760, 1045, and so on in Figure 1, show the average number of hotspots (HSs year⁻¹) of each 1° grid cell. The largest number of HSs is 2415 in the 1° grid cell (17–18° N, 93–94° W) located southwest of Villahermosa in Southeast Mexico (SEM). The number of HSs in this grid cell varied from 1134 (minimum) in 2004 to 4371 (maximum) in 2021. This grid cell had the maximum number of HSs in nine years (2009, 2010, 2012, 2014, and the most recent five years from 2018 to 2022). In Southwest Mexico (SWM), the 1° grid cell (18–19° N, 102–103° W) had the largest number of HSs with 1629 and is a fire center on the Pacific Ocean side.

3.2. Recent Fire History in Mexico

Figure 3a shows recent Mexico fire history from 2003 to 2022. Each annual bar graph in Figure 3a is divided into four to show the fire history of Southwest Mexico (SWM), Southeast Mexico (SEM), Northwest Mexico (NWM), and Northeast Mexico (NEM). Average annual HS values with their percentages are: 70,053 for Mexico, 34,755 (50%) for the SWM, 23,926 (34%) for the SEM, 8637 (12%) for the NWM, and 2736 (4%) for the NEM. Eighty-four percent of fires occurred in areas south of 22° N. The highest number of HSs was 109,329 in 2011 and the lowest was 41,334 in 2014. There was a difference of about 2.6 times.

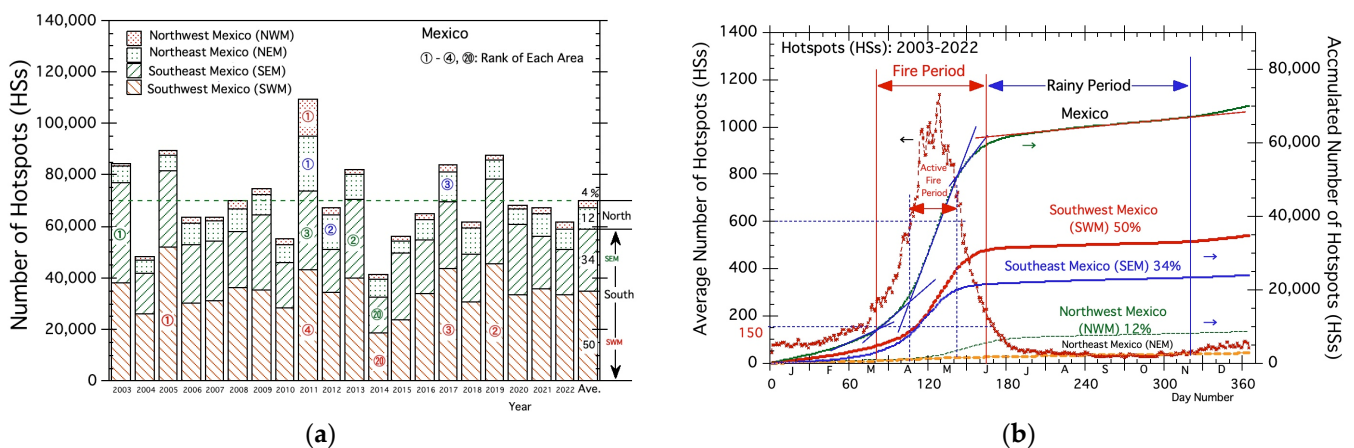


Figure 3. Recent fire history from 2003 to 2022 and average fire period in Mexico. Marks such ①, ②, ... ⑳ show fire ranks in each of the four areas. J: January, F: February, M: March, A: April, M: May, J: June, J: July, A: August, S: September, O: October, N: November, D: December. DN: day number. (a) Annual fire history. (b) Average fire period.

To clarify fire activities in the SWM, the SEM, the NWM, and the NEM, fires were ranked by the number of hotspots (HSs) in each of the four areas, and these are shown by marks such as ①, ② and ⑳. The largest fire (HSs = 109,329) in Mexico occurred in 2011. Fire ranks in the SWM, the SEM, the NWM, and the NEM were 3rd, 4th, 1st, and 1st, respectively.

Figure 3b shows the average annual fire occurrence trend in Mexico. Using the gradients of the five different thin straight lines on the cumulative HSs curve, the average fire duration, average fire activity duration, and average rainfall (low fire) period can be defined, as shown in Figure 3b. The average fire period (defined by HSs > about 150) begins

from around the middle of March and lasts until the middle of June. The average active fire period (HSs > about 600) starts from around the middle of April and lasts until the middle of May.

Four accumulated HS curves for the SWM, the SEM, the NWM, and the NEM show each fire period and fire activity throughout the year. Since 84% of fires occur in southern Mexico, various analyses will be conducted in the next section, primarily on the SWM and the SEM.

3.3. Fire Weather Conditions in Southeast Mexico (SEM)

This section describes the third step in Figure 2. Fire weather conditions were extracted by analyzing the relationship between basic weather parameters such as rainfall, temperature, humidity, wind speed, wind direction, pressure, and weather type measured in Villahermosa, and fire activity in the SEM.

3.3.1. Average Fire and Dry Period in Villahermosa

Using 20 years (from 2003 to 2022) of fire and rainfall data, the average fire occurrence in the SEM is shown in Figure 4a and average daily rainfall in the Villahermosa area is shown in Figure 4b. From daily average HSs changes in Figure 4a, the average fire period and active fire period could be defined using the gradients of the three different thin straight lines on the accumulated HSs curve (thick blue curve). The fire period (HS > about 100) starts around the middle of March and lasts until the end of May. The active fire period (HS > about 260) begins around the middle of April and lasts until the middle of May.

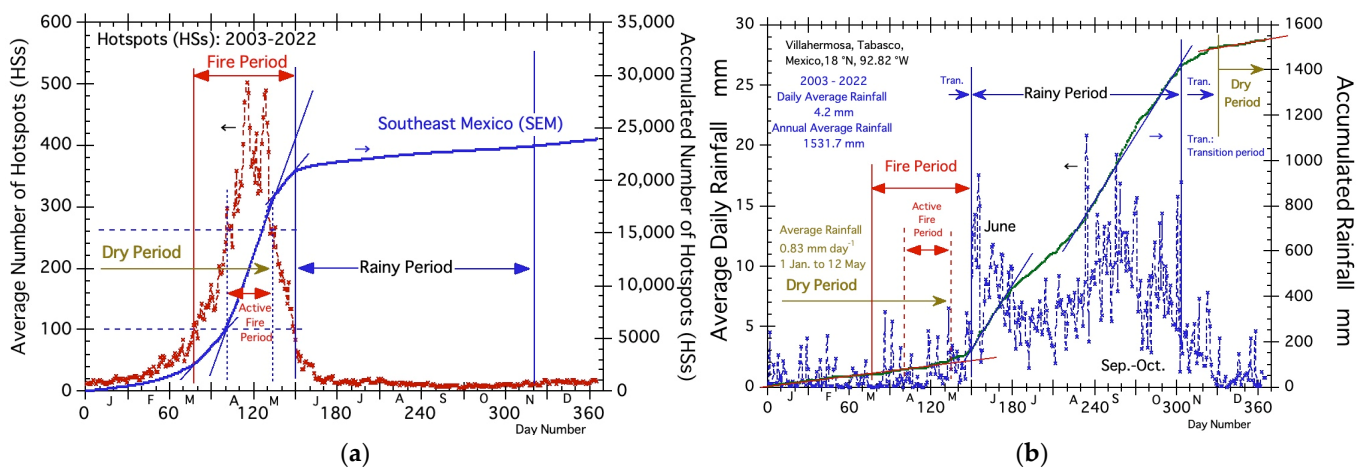


Figure 4. Average fire and active fire period (HSs), and average rainy and dry period in southeastern Mexico (SEM). J: January, F: February, M: March, A: April, M: May, J: June, J: July, A: August, S: September, O: October, N: November, D: December. Tran.: Transition. DN: day number. (a) Average fire and active fire period. (b) Average rainy and dry period.

The fire period (HS > about 100) almost coincides with the brighter period of the year in Villahermosa. According to Weather Spark [37], the brighter (strong solar radiation) period of the year in Villahermosa lasts for 2.3 months, from 9 March to 17 May, with an average daily incident shortwave energy per square meter above 6.3 kWh (peak value is 6.8 kWh on 8 April).

Figure 4b shows average daily rainfall in the Villahermosa area for the 20-year period from 2003. Rainy and dry periods could be defined by gradients of thin straight lines on the accumulated rainfall curve (green curve). The rainy period starts from the beginning of June and lasts until the end of October. The dry period starts from around the beginning of December (of the previous year) and lasts until the middle of May.

3.3.2. Active Fire Period in 2003 (Top Fire Year in the SEM)

Figure 5a,b shows fire occurrence and rainfall trends from January to June in 2003 (top fire year) and 2014 (inactive fire year). Figure 5a shows that fires in 2003 became active from the beginning of March and lasted until the end of May, or just before the average rainy period. These active fires occurred under low rainfall conditions (total 3 mm rainfall from 1 January to 12 May). On the other hand, Figure 5b shows that active fires in 2014 started from the end of March and ended in the middle of May. Total rainfall from January 1 to May 12 in 2003 and 2014 is 3 mm and 215 mm, respectively, as shown in Figure 5. The total rainfall of 3 mm in 2003 suggests that fires in 2003 became active under drought. On the other hand, the total rainfall of 215 mm in 2014, and the large daily rainfalls of 62 mm (8 April (DN (day number) = 98)) and 21 mm (1 May (DN = 121)) in Figure 5b, suggest there were wet conditions in 2014 made by rainfall, and fires in 2014 were not so active as a result.

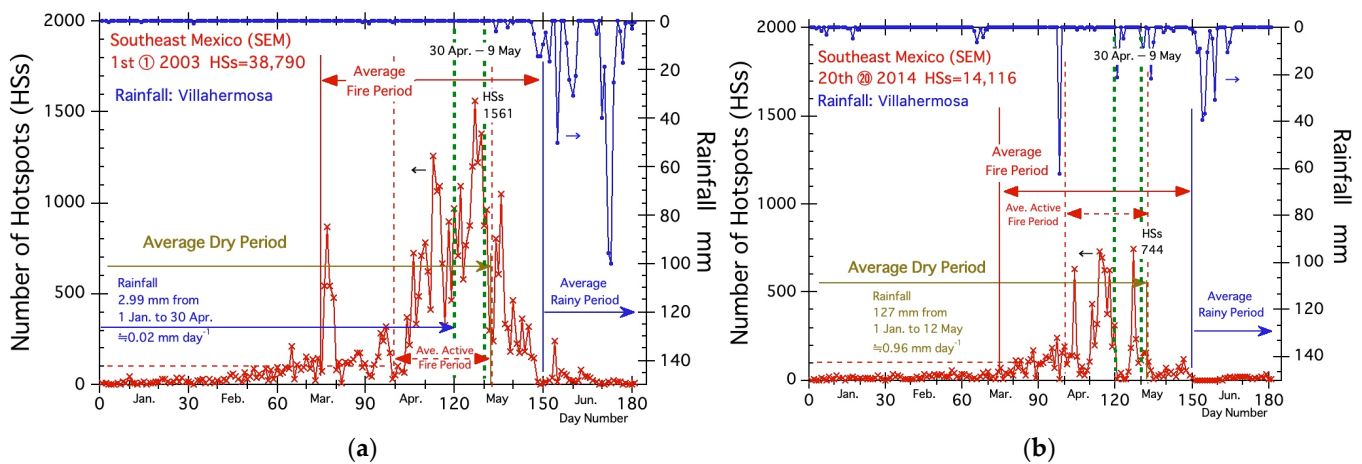


Figure 5. HS (fire) and rainfall in 2003 and 2014. Jan.: January, Feb.: February, Mar.: March, Apr.: April, Jun.: June. Ave.: Average. DN: day number. (a) Fire and rainfall in 2003 (top active fire year). (b) Fire and rainfall in 2014 (inactive fire year).

Based on these results and the fire trends shown in Figure 5a, it was determined that the weather conditions just prior to the onset of rainfall were the most characteristic. Ten days from 30 April to 9 May, including the highest HS peak in 2003 (HSs = 1561) and in 2014 (HSs = 744), were selected for analysis of the weather data. Ten days periods in 2003 and 2014 are shown by two green dashed lines in Figure 5a,b.

3.3.3. Fire Weather Conditions in Villahermosa

In this section, the fire-prone weather conditions from comparing hourly weather data measured at Villahermosa in the SEM during active fire periods in 2003 (top active fire year) and 2014 (inactive fire year) were extracted. This comparison is the main analysis of the third step (3. Analysis of fire weather conditions) in Figure 2. At the Villahermosa weather station, very little nighttime data was measured between 11:00 p.m. and 5:00 am, but this had little impact on the evaluation of the fire-prone weather conditions as they occurred mainly during the afternoon hours.

- Temperature and relative humidity (RH)

Figure 6a shows the daily change of hotspots (HSs) and diurnal changes of temperature during the fire period from 30 April to 9 May in 2003 and 2014. The large morning temperature increases in 2003 (the average increase rate is $2 \text{ }^\circ\text{C h}^{-1}$ (28 °C at 8 a.m. to 32 °C at 10 a.m.)) was due to high incident shortwave energy under fair weather conditions. Maximum temperatures in 2003 are above 37 °C on most days except 30 April. On the other hand, rainfall on 1 and 3 May suggest that the low temperature trend in 2014 (the

average increase rate is $1.24\text{ }^{\circ}\text{C h}^{-1}$ ($24.78\text{ }^{\circ}\text{C}$ at 8 a.m. to $27.15\text{ }^{\circ}\text{C}$ at 10 a.m.)) were mainly due to low incident shortwave energy under rainy and cloudy weather conditions.

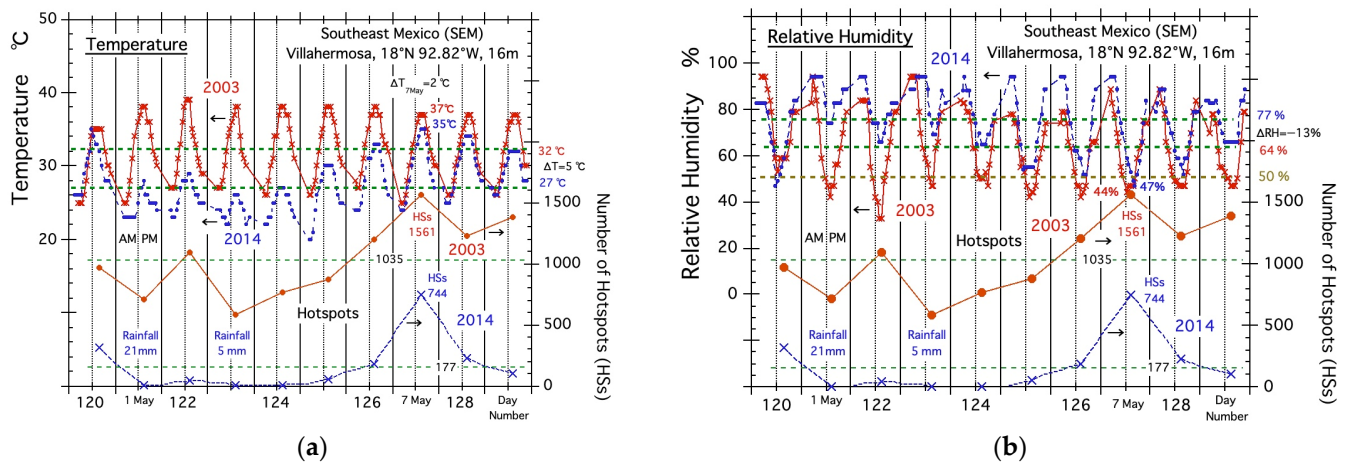


Figure 6. Air temperature and relative humidity (RH) in 2003 and 2014. Red line curves of temperature, RH, and hotspot are for 2003. Blue line curves of temperature, RH, and hotspot are for 2014. DN: day number. (a) Temperature and hotspot. (b) Relative humidity (RH) and hotspot.

The occurrence trend during the active period can be explained to some extent by the difference in average temperatures between 2003 and 2014. In 2003, active fires (average HSs = 1035) lasted under the average temperature of $32\text{ }^{\circ}\text{C}$. On the other hand, in 2014, when the average temperature was lower at $27\text{ }^{\circ}\text{C}$, the average number of HSs was 177, about one-fifth of the above HSs in 2003.

Figure 6b shows hourly changes of relative humidity (RH) during the fire period from 30 April to 9 May in 2003 and 2014. The active fires in 2003 occurred under an average RH of 64%, about 13% lower than the average RH of 77% in 2014. In general, fires tend to become more active as the RH decreases, and it can be said that fires in 2003 became more active when the RH was below 50% during the daytime. This RH trend can also be seen from 6 to 8 May in 2014. On 7 May (the peak fire day), where fires became active when their minimum RH was less than 50%, as shown in Figure 6b.

- Wind speed and wind direction

Figure 7a shows hourly changes in wind speed during the fire period from 30 April to 9 May in 2003 and 2014. The active fires in 2003 occurred under the average wind speed of 10.3 km h^{-1} , about 2.6 km h^{-1} (difference in average wind speed between the two years, ΔV) faster than the average wind speed of 7.6 km h^{-1} in 2014. This difference in the number of fires (HSs) due to wind speed seems to suggest that fires in the SEM are also wind speed dependent. The average wind speed on 7 May, the day of the largest fire (HSs = 1561 and 744), was 12.3 km h^{-1} in 2003 and 7.6 km h^{-1} in 2014. The difference in wind speed averages (ΔV) is 4.7 km h^{-1} . The maximum wind speed on 7 May was 17 km h^{-1} in 2003 and 24 km h^{-1} in 2014. Active fires in 2003 occurred under relatively a higher wind speed of 10.3 km h^{-1} .

Figure 7b shows the hourly changes in wind direction during the fire period from 30 April to 9 May in 2003 and 2014. Figure 7b shows active fires in 2003 occurred under mainly easterly winds of NE and E. This easterly wind direction is suggesting that it is the predominant fire wind direction. Wind direction changes in 2014 in Figure 7b will support “fire wind direction”. In 2014, wind direction changed from westerly wind (SW and NW) on 4 May to easterly wind (NE and N) on 5 May. Under easterly wind, fires in 2014 became active on May 7 and the number of HSs exceeded 700 (744, Figure 5b). Fires, both in 2003 and 2014, became active under easterly wind (average 72° in 2003 and 84° in 2014) from 5 May. As average wind directions in May in Villahermosa are 45% North, 35%

East, 10% West, and 10% South [37], easterly wind ($\approx 90^\circ$) could be the fire wind direction in Villahermosa.

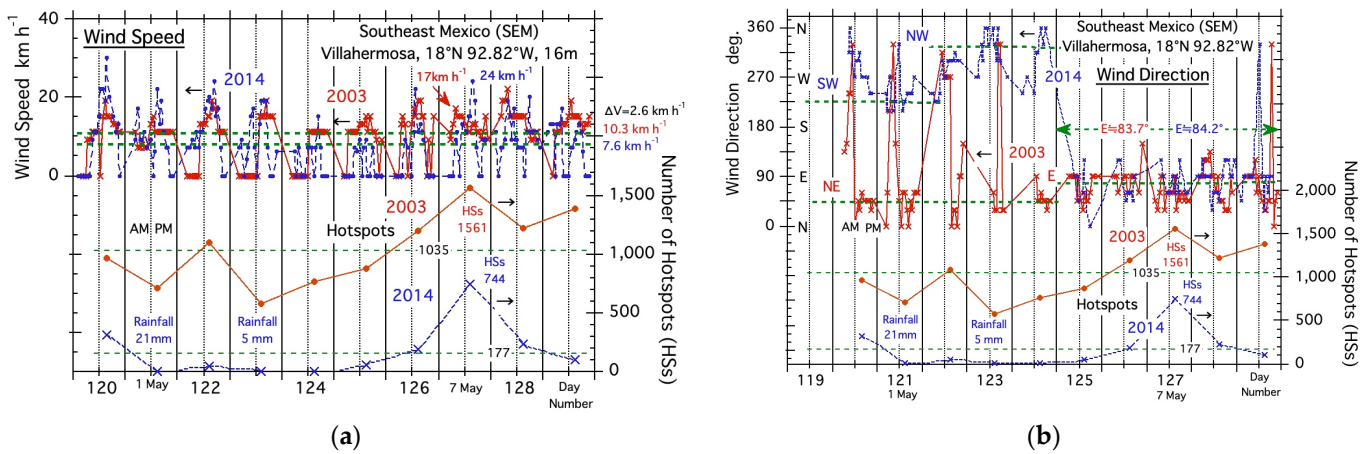


Figure 7. Wind speed direction and hotspots in 2003 and 2014. N: North, W: West, S: South, E: East, SW: Southwest, NW: Northwest, NE: Northeast. DN: day number. (a) Wind speed and hotspots. (b) Wind direction and hotspots.

The high afternoon wind speed in Figure 7a and the wind direction (easterly ($\approx 90^\circ$)) in Figure 7b suggest that the “sea breeze” from the Caribbean is blowing due to the formation of a thermal low (or thermocline) [38]. High temperatures ($>35^\circ\text{C}$) in the afternoon in Figure 6a support the formation of a thermal low (or heat low).

- Air pressure

Figure 8 shows hourly changes in air pressure during the fire period from 30 April to 9 May in 2003 and 2014. The active fires in 2003 occurred under the low air pressure of 1005.6 hPa, about -5.8 hPa (difference in average air pressure between the two years, ΔP) lower than the average air pressure of 1011.4 hPa in 2014. This difference in the number of fires (HSs) due to air pressure seems to suggest that fires in the SEM are air pressure dependent. The average air pressure on 7 May, the day of the largest fire (HSs = 1561 and 744), was 1005 hPa in 2003 and 1008.4 hPa in 2014. Difference in air pressure averages (ΔV) is -3.4 hPa. The maximum air pressure on 7 May was 1006.9 hPa in 2003 and 1010.6 hPa in 2014. Afternoon pressure drops ($<$ about 1006 hPa) on most days suggests the development of a “thermal low”. Summing up the above trends in air pressure and fire, we may say that the threshold level may be about 1010 hPa.

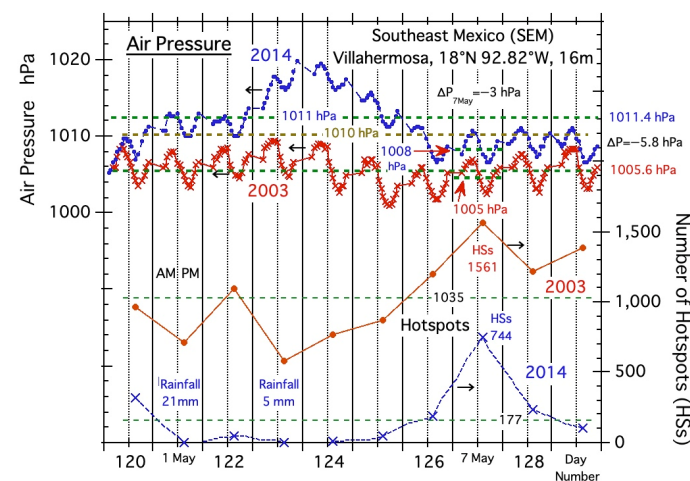


Figure 8. Air pressure and hotspots in 2003 and 2014. DN: day number.

- Weather type

The frequency of weather types (fair, cloudy, rainy, etc.) per day during the 2003 and 2014 fire periods (30 April to 9 May) is shown in Figure 9. Figure 9a shows that the weather type in 2003 is mostly “Fair” (average frequency is 16). Percentage of “Fair” is 90.4% ($16/17.7 \times 100 = 90.4$, without deficit). On the other hand, as shown in Figure 9b, “Fair” in 2014 is small at 13.2% ($2.6/19.7 \times 100 = 13.2$) on average. As active fires on 7 May 2014 occurred under “Fair” and “Partly Cloudy” (their frequency was 18 ($18/20 \times 100 = 90\%$)), we may say “Fair” weather is one of the weather types necessary for active fires in Villahermosa.

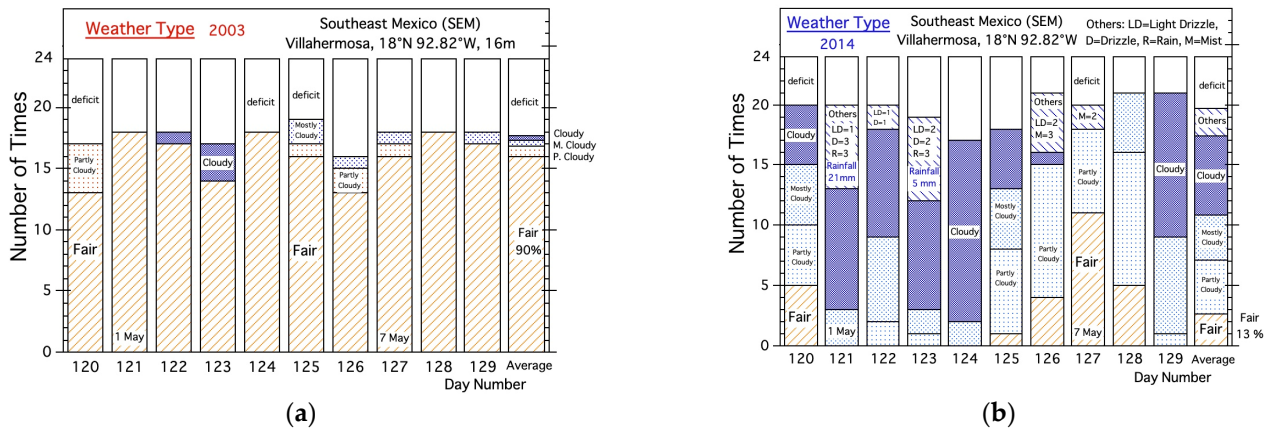


Figure 9. Weather type in 2003 and 2014. DN: day number. (a) Weather type in 2003. (b) Weather type in 2014.

3.4. Fire Weather Conditions in Southwest Mexico (SWM)

This section describes the third step in Figure 2. Fire weather conditions are extracted by analyzing the relationship between basic weather parameters such as rainfall, temperature, humidity, wind speed, wind direction, pressure, and weather type measured in Colima, and fire activity in the SWM.

3.4.1. Average Fire and Dry Period in Colima

Using 20 years (from 2003 to 2022) of fire and rainfall data, the average fire occurrence in SWM is shown in Figure 10a and average daily rainfall at Colima area is shown in Figure 10b. From the daily average HSs change in Figure 10a, the average fire period and active fire period could be defined using the gradients of the three different thin straight lines on the accumulated HSs curve (thick green curve).

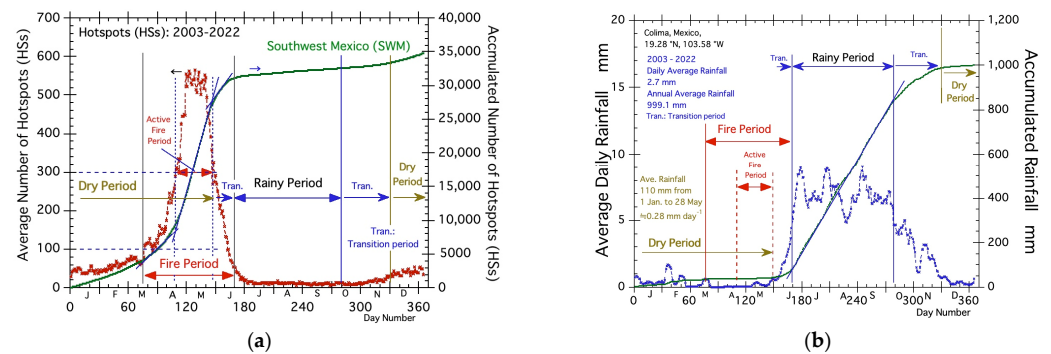


Figure 10. Average fire and active fire period (HSs), and average rainy and dry period in southwestern Mexico (SWM). J: January, F: February, M: March, A: April, M: May, J: June, J: July, A: August, S: September, O: October, N: November, D: December. Tran.: Transition. DN: day number. (a) Average fire and active fire period. (b) Average rainy and dry period.

The average fire period (defined by HSs > about 100) begins from around the middle of March and lasts until the end of May. Active fire period could be defined by gradients of thin straight lines on the accumulated HSs curve (thick green curve). The active fire period (HSs > about 300) starts from around the end of April and lasts until the end of May.

The fire period (HS > 100) almost coincides with the brighter period of the year in Colima. According to Weather Spark [39], the brighter (strong solar radiation) period of the year in Colima lasts for 2.5 months, from 13 March to 31 May, with an average daily incident shortwave energy per square meter above 7.2 kWh (peak value is 7.3 kWh on 6 May).

Figure 10b shows average daily rainfall in the Colima area for the 20-year period starting from 2003. The rainy and dry period could be defined by gradients of thin straight lines on the accumulated rainfall curve (green curve). The rainy season begins at the end of June and lasts until the beginning of October. Dry period starts from around the beginning of December (of the previous year) and lasts until the middle of May. The average annual rainfall in Colima is 999.1 mm, which is less than the 1531.7 mm rainfall in Villahermosa (see Figure 4b).

3.4.2. Active Fire Period in 2005 (Top Fire Year in SWM)

Figure 11a,b shows fire occurrence and rainfall trends from January to June in 2005 (top fire year) and 2014 (inactive fire year). Figure 11a shows that fires in 2005 became active from the middle of March and lasted until the middle of June or just before the average rainy period. On the other hand, Figure 11b shows that active fires in 2014 started from the middle of April and ended at the beginning of June. To explain different fire activities for both years, various weather conditions were analyzed in the next section. I selected the 10 day period of 1–10 May during the active fire period from the end of April to the end of May which include highest HSs peak (HSs = 1262) in 2005. The 10 day periods in 2005 and 2014 are shown by green dashed lines in Figure 11a,b.

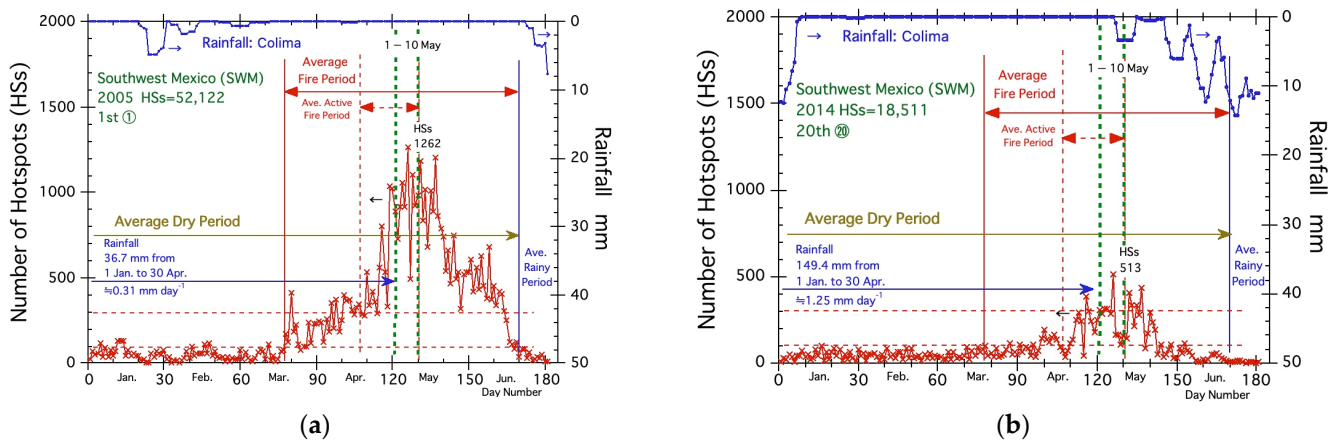


Figure 11. HS (fire) and rainfall in 2005 and 2014. Jan.: January, Feb.: February, Mar.: March, Apr.: April, Jun.: June. Ave.: Average. DN: day number. (a) Fire and rainfall in 2005 (top active fire year). (b) Fire and rainfall in 2014 (inactive fire year).

3.4.3. Fire Weather Conditions in Colima

In this section, I discuss the fire weather conditions by comparing hourly weather data measured in Colima in SWM during active fire periods in 2005 (top active fire year) and 2014 (inactive fire year). This comparison is the main analysis of the third step (3. Analysis of fire weather conditions) in Figure 2. At the Colima weather station, very little nighttime data was measured between 11:00 p.m. and 5:00 a.m., but this had little impact on the evaluation of the fire-prone weather conditions, as they occurred at mainly afternoon hours after 12:00 p.m.

- Temperature and relative humidity

Figure 12a shows the daily change of hotspots (HSs) and diurnal changes of temperature during the fire period from 1 to 10 May in 2005 and 2014. The large morning temperature increases in 2005 (the average increase rate is $1.84\text{ }^{\circ}\text{C h}^{-1}$ ($23.10\text{ }^{\circ}\text{C}$ at 8 a.m. to $26.78\text{ }^{\circ}\text{C}$ at 10 a.m.)) will be mainly due to high incident shortwave energy under fair weather conditions. Maximum temperatures of most days in 2005 exceeded $30\text{ }^{\circ}\text{C}$. On the other hand, rainfall from May 8 to 10 in 2014 suggests that the low temperature trend (the average increase rate is $1.20\text{ }^{\circ}\text{C h}^{-1}$ ($24.00\text{ }^{\circ}\text{C}$ at 8 a.m. to $25.40\text{ }^{\circ}\text{C}$ at 10 a.m.)) was due to low incident shortwave energy under rainy and cloudy weather conditions.

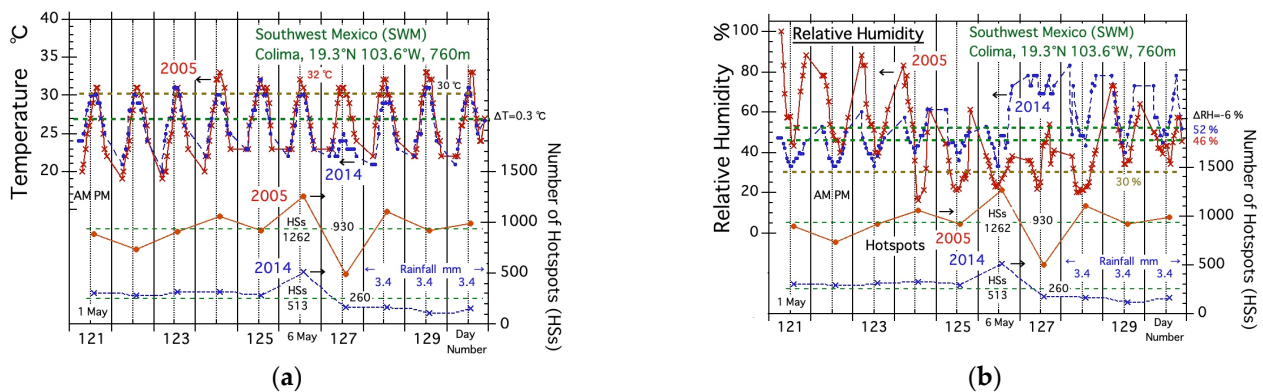


Figure 12. Air temperature and relative humidity (RH) in 2005 and 2014. Red line curves of temperature, RH, and hotspots are for 2005. Blue line curves of temperature, RH, and hotspots are for 2014. DN: day number. (a) Temperature and hotspots. (b) Relative humidity (RH) and hotspots.

Figure 12b shows hourly changes of relative humidity (RH) during the fire period of 1–10 May in 2005 and 2014. The active fires in 2005 occurred under an average RH of 46%, about 6% lower than the average RH of 52% in 2014. In general, fires tend to become more active as the RH decreases, and it can be said that fires in 2005 became more active when the RH was below 40% during the daytime. This RH trend can also be seen from 1–6 May 2014. On 6 May (the maximum fire day), fires became very active when their minimum RH was less than 30%, as shown in Figure 12b. These active fire occurrences under low RH suggest RH is one of the most sensitive weather parameters for Colima.

- Wind speed and wind direction

Figure 13a shows hourly changes of wind speed during the fire period of 1–10 May in 2005 and 2014. From Figure 13a, we can see that the wind speed in the morning is weak and mostly 0 km h^{-1} (calm), and in the afternoon the wind speed tends to increase (over 17 km h^{-1}). Strong wind in the afternoon may indicate that sea breezes are blowing. Under strong sea breezes (over 23 km h^{-1}), the average number of HSs is 260, even in the lowest fire year, 2014. The maximum wind speeds on 6 May, the day of the largest fire (HSs = 1262 and 513), were 28 km in 2005 and 33 km in 2014.

Figure 13b shows hourly changes of wind direction during fire period of 1–10 May in 2005 and 2014. Wind directions of sea breezes in the afternoon are mostly WSW (241° in 2005 and 237° in 2014) as shown in Figure 13b. Wind directions of maximum wind speeds on 6 May, 28 and 33 km h^{-1} in 2005 and 2014, were also mostly WSW. As average wind directions in May in Colima are 45% North, 35% East, 10% West, and 10% [39], southwesterly wind WSW (241°) could be the fire wind direction in Colima.

- Air pressure

Figure 14 shows hourly changes of air pressure during the fire period of 1–10 May in 2005 and 2014. There was no significant difference in air pressure. Although the difference in average air pressure is small, it can be said that fires in 2005 and 2014 occurred under atmospheric pressure lower than about 935 hPa.

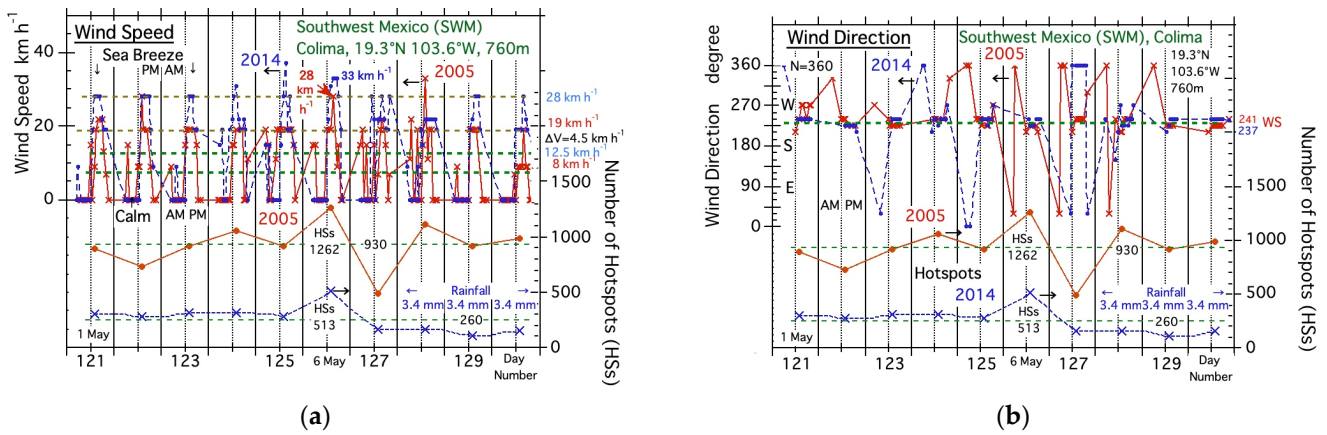


Figure 13. Wind speed and wind direction in 2005 and 2014. N: North, W: West, S: South, E: East, SW: Southwest, NW: Northwest, NE: Northeast. DN: day number. (a) Wind speed and hotspots. (b) Wind direction and hotspots.

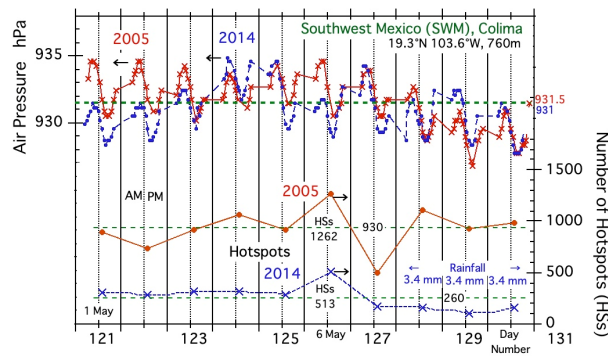


Figure 14. Air pressure in 2005 and 2014. As data in 2005 has large pressure drop data (about 10 hPa h^{-1}), 27 data below 927 hPa (lowest pressure was 916.16 hPa at 6 a.m. on 10 May) were not plotted. DN: day number.

- Weather type

The frequency of weather types per day during the 2005 and 2014 fire periods (1–10 May) is shown in Figure 9. Figure 15a shows that the weather type in 2005 is mostly “Fair” (average frequency is 11.1). Percentage of “Fair” is 75.5% ($11.1/14.7 \times 100 = 75.5$, without deficit). On the other hand, as shown in Figure 15b, “Fair” in 2014 is small at 7.8% ($1.2/15.3 \times 100 = 7.8$) on average. As active fires on 6 May 2014 occurred under “Fair” and “Partly Cloudy” (their frequency was 11 ($(4 + 7)/16 \times 100 = 68.8\%$)), we may say “Fair” weather type is one of the weather types necessary for active fires in Colima as well as Villahermosa in the SEM.

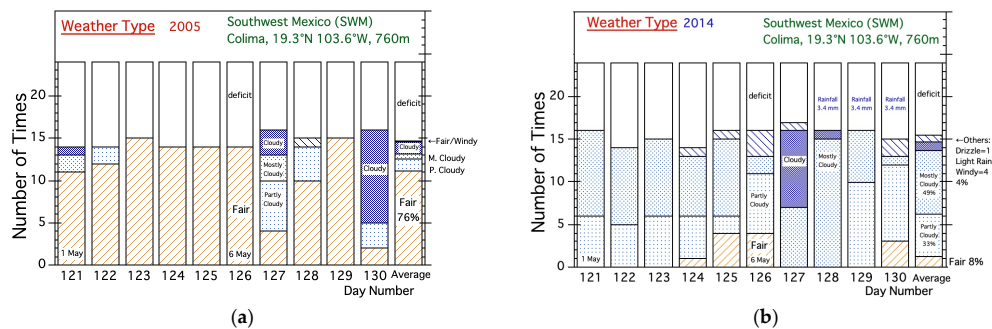


Figure 15. Weather type in 2005 and 2014. DN: day number. (a) Weather type in 2005. (b) Weather type in 2014.

4. Discussion

4.1. Forest Fire Researches in Mexico

Several papers have already been published regarding fires in Mexico. L. Galván and V. Magaña proposed the probability estimation model of forest fires in Mexico using information on precipitation and temperature, along with data on the type of vegetation, human activities near forests, and fire prevention policies [40]. R. M. Domínguez, D. A. R. Trejo reported: the number of forest fires in Mexico has increased in recent decades and their environmental, economic, and social costs are significant [41]. One of their conclusions is that “the combination of these factors and hazard data results in a model that better explains probabilities of forest fires than the approach based on climate information only” [41]. The above two papers use probability theory to assess fires in Mexico and attempt to prepare for future fires. However, extreme phenomena such as floods caused by heavy rain and prolonged droughts have already occurred in several countries and regions, so it is important to prepare for fires with unprecedented magnitude in Mexico. In other words, in addition to the results of probability theory, it is necessary to clarify fire weather conditions and fire-related climate indices for Mexican fires.

4.2. Fire-Prone Weather Conditions in the SEM and the SWM

Typical fire-prone weather conditions for Southeast Mexico (SEM) and Southwest Mexico (SWM) were discussed in Sections 3.3 and 3.4 respectively. Two “sea breezes” with different wind directions played important roles in SEM and SWM. A detailed analysis of fires in the mountain areas of Mexico is also very important [42]. However, detailed analysis of fire activity was difficult without several local weather data. Instead, the Great Divide needed for a synoptic analysis is shown in Figure 1. Major fire-prone weather conditions are briefly summarized below.

In Southeast Mexico (SEM): Based on the analysis of the weather data for SEM shown in Figures 5–9, we can say that active fires are occurring in the SEM under conditions of continuous sunny days and air pressure less than about 1010 hPa, maximum temperatures above 32 °C and relative humidity less than about 50%, and strong easterly wind ($\approx 90^\circ$). Temporal changes in these meteorological data suggest that fires occur under fire meteorological conditions caused by sea breezes blowing from the Caribbean. Finally, among the above meteorological parameters, “temperature” had the largest difference ($\Delta T = 5^\circ\text{C}$ in Figure 6a), so we may say that “temperature” is the most sensitive fire weather parameter for the SEM.

In Southwest Mexico (SWM): Based on the analysis of the weather data for the SWM shown in Figures 11–15, we can say that active fires are occurring in the SWM under conditions of continuous sunny days, air pressure less than about 930 hPa, maximum temperatures above 30 °C and relative humidity less than about 46%, and strong south-westerly wind ($\approx 240^\circ$). Temporal changes in these meteorological data suggest that fires occur under fire meteorological conditions caused by sea breezes blowing from the Pacific Ocean. Finally, among the above meteorological parameters, “relative humidity (RH)” had the largest difference ($\Delta RH = -6\%$ in Figure 12b), so we may say that “relative humidity” is the most sensitive fire weather parameter for the SWM.

4.3. Fire-Related Indices for the SEM and SWM

This section describes the final steps (4. Selection and evaluation of fire-related indices) shown in Figure 2. The best fire-related indices that can adequately assess fire activity for each year is selected from among NOAA’s main indicators (see caption for Figure 2). The correlation between each index value and the total number of fires during the fire period is examined.

4.3.1. Fire-Related Index for the SEM

Air temperature anomaly (TA) and outgoing longwave radiation anomaly (OLRA) are introduced to describe air and surface temperature conditions related to “temperature” (the

most sensitive fire weather parameter for the SEM). TA in Figure 16a had the coefficient of determination (R^2) value of 0.7579.

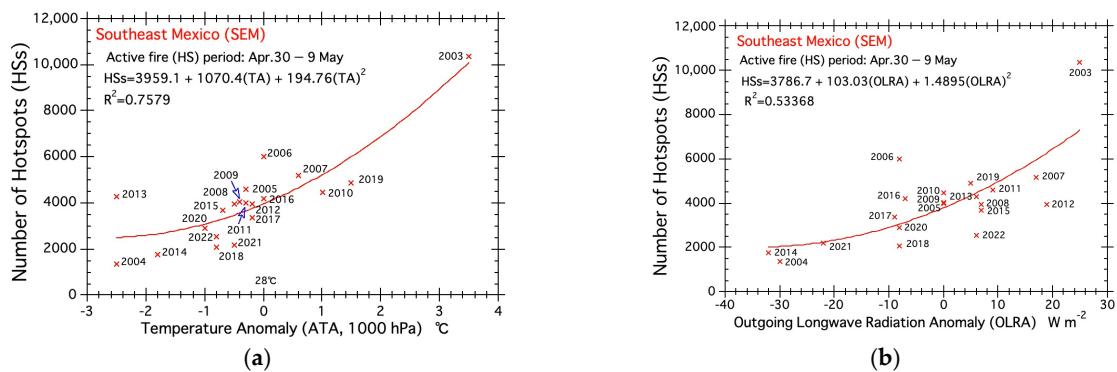


Figure 16. Fire-related indices for the SEM. (a) Temperature anomaly (TA). (b) Outgoing longwave radiation anomaly (OLRA).

OLR is a measure of the amount of energy emitted to space by earth’s surface, oceans, and atmosphere (The National Center for Atmospheric Research (NCAR) climate data guide (<https://climatedataguide.ucar.edu/climate-data/outgoing-longwave-radiation-olr-hirs>, accessed on 13 December 2023)). OLRA in Figure 16b had the coefficient of determination (R^2) value of 0.53368.

The above relatively high R^2 values suggest fires in the SEM simply depend on air and surface temperatures of inland areas in the SEM. R^2 of other indices are low and non-correlated like Nino 3 ($R^2 = 0.011825$), Nino 4 ($R^2 = 0.018907$), and POD ($R^2 = 0.0058714$).

4.3.2. Fire-Related Index for the SWM

Based on the analysis of the weather data for the SWM shown in Figures 11–15, we can say that active fires are occurring in the Southwest Mexico (SWM) under conditions of continuous sunny days and air pressure less than about 930 hPa, maximum temperatures above 30 °C and relative humidity less than about 50%, and strong southwesterly winds ($\approx 230^\circ$). Temporal changes in these meteorological data suggest that fires occur under fire meteorological conditions caused by sea breezes blowing from the Caribbean. Precipitable water vapor (PWV) is introduced to describe dry conditions related to “relative humidity” (the most sensitive weather parameter for the SWM).

PWV is the vertically integrated amount of water vapor in the atmosphere and is a valuable index for weather forecasting [43]. The precipitable water vapor anomaly (PWVA) was already used to explain tropical peatland fires in Central Kalimantan [34].

The index, PWVA shown in Figure 17, had a good negative correlation (the coefficient of determination (R^2) value is 0.7683). R^2 of other indices are low and non-correlated (Nino 3 ($R^2 = 0.12925$), Nino 4 ($R^2 = 0.024794$), POD ($R^2 = 0.10491$)).

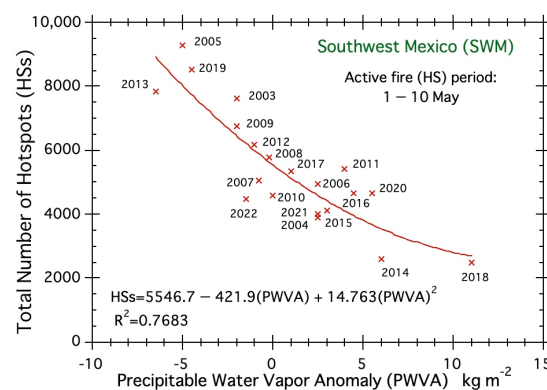


Figure 17. Fire-related indices for the SWM.

5. Conclusions

Fire conditions in Mexico were carefully analyzed using 20 years of satellite hotspot and rainfall data, hourly weather data, and various satellite data to determine fire weather conditions and fire-related indices. The main conclusions drawn from the analysis are summarized below:

- (1) The majority of fires in Mexico (approximately 84%) occur mainly in areas south of the Tropic of Cancer.
- (2) Southwest Mexico (the SWM, $N < 22^\circ$, $94\text{--}106^\circ$ W) and Southeast Mexico (the SEM, $N < 22^\circ$, $86\text{--}94^\circ$ W) account for 50% and 34% of all fires in Mexico, respectively.
- (3) Analysis results using hourly data showed that westerly wind sea breezes from the Pacific Ocean blow toward the coastal land areas of the SWM. Easterly sea breezes from the Caribbean blow into the land area of the SEM.
- (4) Fires in the SWM and the SEM became active under high temperatures, low relative humidity, high wind speed, low air pressure, and fair weather. The most sensitive fire weather parameters were “relative humidity” for the SWM and “temperature” for the SEM.
- (5) Based on the analysis results, the fire-related indices selected were “precipitable water vapor anomaly (PWVA)” for the SWM and “temperature anomaly (TA)” for the SEM.
- (6) The SWM fire index (PWVA) suggests that future fires will depend on dryness, while the SEM fire index (TA) suggests that future fires will depend on high temperature trends.

Lastly, I do hope that the results of this paper will improve local fire forecasts and help analyze future fire trends under global warming in Mexico. Since the proposed method obtains all fire-related data necessary for analysis from the Internet, I hope that the analytical methods and procedures in this paper will be applied to fire analysis in other fire-prone countries and regions.

Funding: This research received no external funding.

Institutional Review Board Statement: Not applicable.

Informed Consent Statement: Not applicable.

Data Availability Statement: All data used in this paper are publicly available on the Internet. Fire (Hotspot) data: MODIS Collection 6.1, <https://firms2.modaps.eosdis.nasa.gov/download/>. Rainfall data: JAXA, https://sharaku.eorc.jaxa.jp/GSMaP_CLM/index.htm. Hourly weather data: Weather underground, Villahermosa: <https://www.wunderground.com/history/daily/mx/centro/MMVA/>, Colima: <https://www.wunderground.com/history/daily/mx/cuauhtemoc/MMIA/date/2020-5-16>. NCEP/NCAR 40-year reanalysis data: <https://psl.noaa.gov/data/composites/day/>. Climate data (Climate and Average Weather Year Round): Colima, <https://weatherspark.com/y/3823/Average-Weather-in-Colima-Mexico-Year-Round>, Villahermosa, <https://weatherspark.com/y/10690/Average-Weather-in-Villahermosa-Mexico-Year-Round> (all accessed on 1 October 2023).

Acknowledgments: I would like to thank the following institutes and various earth data sites: (1) various weather maps from the Twentieth Century Reanalysis Project version 3 dataset provided by the U.S. Department of Energy, Office of Science Biological and Environmental Research (BER), by the National Oceanic and Atmospheric Administration Climate Program Office, and by the NOAA Physical Sciences Laboratory. (2) rainfall data from the JAXA (https://sharaku.eorc.jaxa.jp/GSMaP_CLM/index.htm, accessed on 1 October 2023). (3) hourly weather data from weather underground (<https://www.wunderground.com/history/daily/my/malacca/WMKM/date/2019-3-6>, accessed on 11 August 2023). (4) various maps from Google Map Pro by Google LLC. (5) various imagery from NASA’s Worldview application (<https://worldview.earthdata.nasa.gov>, accessed on 1 October 2023), part of NASA’s Earth Observing System Data and Information System (EOSDIS). (6) climate data form “Climate and Average Weather Year Round” (Weather Spark, <https://weatherspark.com/y/3823/Average-Weather-in-Colima-Mexico-Year-Round> (accessed on 1 October 2023)).

Conflicts of Interest: The authors declare no conflicts of interest.

References

1. UN Environment Programme. UN Report Spreading Like Wildfire/The Rising Threat. Available online: <https://www.unep.org/resources/report/spreading-wildfire-rising-threat-extraordinary-landscape-fires> (accessed on 13 December 2023).
2. Benali, A.; Mota, B.; Carvalhais, N.; Oom, D.; Miller, L.M.; Campagnolo, M.L.; Pereira, J.M.C. Bimodal fire regimes unveil a global-scale anthropogenic fingerprint. *Glob. Ecol. Biogeogr.* **2017**, *26*, 799–811. [\[CrossRef\]](#)
3. Morton, D.C.; Defries, R.S.; Randerson, J.T.; Giglio, L.; Schroeder, W.; VAN DER Werf, G.R. Agricultural intensification increases deforestation fire activity in Amazonia. *Glob. Chang. Biol.* **2008**, *14*, 2262–2275. [\[CrossRef\]](#)
4. Ward, D.S.; Kloster, S.; Mahowald, N.M.; Rogers, B.M.; Randerson, J.T.; Hess, P.G. The changing radiative forcing of fires: Global model estimates for past, present and future. *Atmos. Chem. Phys.* **2012**, *12*, 10857–10886. [\[CrossRef\]](#)
5. Cochrane, M.A. *The Origins and Control of Forest Fires in the Tropics*; London School of Economics and Political Science, Suntory and Toyota: London, UK, 2021.
6. Cochrane, M.A.; Schulze, M.D. Forest fires in the Brazilian Amazon. *Conserv. Biol.* **1998**, *12*, 948–950. [\[CrossRef\]](#)
7. UNEP. 2002. Available online: <https://www.unep.org/resources/report/unep-annual-report-2002> (accessed on 13 December 2023).
8. Pan, Y.; Chen, J.M.; Birdsey, R.; McCullough, K.; He, L.; Deng, F. Age structure and disturbance legacy of North American forests. *Biogeosciences* **2011**, *8*, 715–732. [\[CrossRef\]](#)
9. Langner, A.; Miettinen, J.; Siegert, F. Land cover change 2002–2005 in Borneo and the role of fire derived from MODIS imagery. *Glob. Chang. Biol.* **2007**, *13*, 2329–2340. [\[CrossRef\]](#)
10. Hoschilo, A.; Page, S.E.; Tansey, K.J.; Rieley, J.O. Effect of repeated fires on land-cover change on peatland in southern Central Kalimantan, Indonesia, from 1973 to 2005. *Int. J. Wildland Fire* **2011**, *20*, 578–588. [\[CrossRef\]](#)
11. Miettinen, J.; Shi, C.; Liew, S.C. Deforestation rates in insular Southeast Asia between 2000 and 2010. *Glob. Chang. Biol.* **2011**, *17*, 2261–2270. [\[CrossRef\]](#)
12. Hooijer, A.; Page, S.; Jauhiainen, J.; Lee, W.A.; Lu, X.X.; Idris, A.; Anshari, G. Subsidence and carbon loss in drained tropical peatlands. *Biogeosciences* **2012**, *9*, 1053–1071. [\[CrossRef\]](#)
13. Page, S.E.; Rieley, J.O.; Banks, C.J. Global and regional importance of the tropical peatland carbon pool. *Glob. Chang. Biol.* **2011**, *17*, 798–818. [\[CrossRef\]](#)
14. Dargie, G.C.; Lewis, S.L.; Lawson, I.T.; Mitchard, E.T.A.; Page, S.E.; Bocko, Y.E.; Ifo, S.A. Age, extent and carbon storage of the central Congo Basin peatland complex. *Nature* **2017**, *542*, 86–90. [\[CrossRef\]](#) [\[PubMed\]](#)
15. Rieley, J. Mega Rice Project (MRP) Central Kalimantan. Available online: <https://peatlands.org/is-indonesia-heading-foranother-mega-rice-project-disaster/> (accessed on 11 March 2023).
16. Aragão, L.E.O.C.; Anderson, L.O.; Fonseca, M.G.; Rosan, T.M.; Vedovato, L.B.; Wagner, F.H.; Silva, C.V.J.; Silva Junior, C.H.L.; Arai, E.; Aguiar, A.P.; et al. 21st Century drought-related fires counteract the decline of Amazon deforestation carbon emissions. *Nat. Commun.* **2018**, *9*, 536. [\[CrossRef\]](#)
17. Libonati, R.; Belém, L.B.C.; Rodrigues, J.A.; Santos, F.L.M.; Sena, C.A.P.; Pinto, M.M.; Filippine, L.; Carvalho, I.A. *Sistema ALARMES—Alerta de Área Queimada Pantanal, Situação Final de 2020. Nota Técnica 01/2021*; Laboratório de Aplicações de Satélites Ambientais: Rio de Janeiro, Brazil, 2021. [\[CrossRef\]](#)
18. Geirinhas, J.L.; Trigo, R.M.; Libonati, R.; Coelho, C.A.; Palmeira, A.C. Climatic and synoptic characterization of heat waves in Brazil. *Int. J. Climatol.* **2018**, *38*, 1760–1776. [\[CrossRef\]](#)
19. Panisset, J.S.; Libonati, R.; Gouveia, C.M.; Machado-Silva, F.; França, D.A.; França, J.R.; Peres, L.F. Contrasting patterns of the extreme drought episodes of 2005, 2010 and 2015 in the Amazon Basin. *Int. J. Climatol.* **2018**, *38*, 1096–1104. [\[CrossRef\]](#)
20. Machado-Silva, F.; Libonati, R.; de Lima, T.F.M.; Peixoto, R.B.; França, J.R.d.A.; Magalhães, M.d.A.F.M.; Santos, F.L.M.; Rodrigues, J.A.; DaCamara, C.C. Drought and fires influence the respiratory diseases hospitalizations in the Amazon. *Ecol. Indic.* **2020**, *109*, 105817. [\[CrossRef\]](#)
21. Junior, C.H.L.S.; Aragão, L.E.O.C.; Fonseca, M.G.; Almeida, C.T.; Vedovato, L.B.; Anderson, L.O. Deforestation-Induced Fragmentation Increases Forest Fire Occurrence in Central Brazilian Amazonia. *Forests* **2018**, *9*, 305. [\[CrossRef\]](#)
22. Bistinas, I.; Harrison, S.P.; Prentice, I.C.; Pereira, J.M.C. Causal relationships versus emergent patterns in the global controls of fire frequency. *Biogeosciences* **2014**, *11*, 5087–5101. [\[CrossRef\]](#)
23. Staver, A.C.; Archibald, S.; Levin, S.A. The global extent and determinants of savanna and forest as alter-native biome states. *Science* **2011**, *334*, 230–232. [\[CrossRef\]](#)
24. Aleman, J.C.; Fayolle, A. Long-term vegetation change in Central Africa: The need for an integrated management framework for forests and savannas. In *Sustainability Challenges in Sub-Saharan Africa I: Continental Perspectives and Insights from Western and Central Africa*; Science for Sustainable Societies, Series; Gasparatos, A., Ahmed, A., Naidoo, M., Karanja, A., Fukushi, K., Saito, O., Takeuchi, K., Eds.; Springer: Singapore, 2020; Chapter 9; pp. 281–315. [\[CrossRef\]](#)
25. Alvarado, S.T.; Andela, N.; Silva, T.S.F.; Archibald, S. Thresholds of fire response to moisture and fuel load differ between tropical savannas and grasslands across continents. *Glob. Ecol. Biogeogr.* **2019**, *29*, 331–344. [\[CrossRef\]](#)
26. VAN Wilgen, B.; Govender, N.; Biggs, H.; Ntsala, D.; Funda, X. Response of Savanna Fire Regimes to Changing Fire-Management Policies in a Large African National Park. *Conserv. Biol.* **2004**, *18*, 1533–1540. [\[CrossRef\]](#)
27. Jia, G.; Shevliakova, E.; Artaxo, P.; De Noblet-Ducoudré, N.; Houghton, R.; House, J.; Kitajima, K.; Lennard, C.; Popp, A.; Sirin, A.; et al. Land–Climate Interactions. In *Climate Change and Land: An IPCC Special Report on Climate Change, Desertification, Land*

- Degradation, Sustainable Land Management, Food Security, and Greenhouse Gas Fluxes in Terrestrial Ecosystems*; Shukla, P.R., Skea, J., Buendia, E.C., Masson-Delmotte, V., Pörtner, H.-O., Roberts, D.C., Zhai, P., Slade, R., Connors, S., van Diemen, R., et al., Eds.; 2019; *in press*; Available online: https://www.ipcc.ch/site/assets/uploads/2019/11/05_Chapter-2.pdf (accessed on 1 October 2023).
28. Hayasaka, H.; Tanaka, H.L.; Bieniek, P.A. Synoptic-scale fire weather conditions in Alaska. *Polar Sci.* **2016**, *10*, 217–226. [[CrossRef](#)]
 29. Hayasaka, H.; Yamazaki, K.; Naito, D. Weather Conditions and Warm Air Masses during Active Fire-periods in Boreal Forests. *Polar Sci.* **2019**, *22*, 100472. [[CrossRef](#)]
 30. Hayasaka, H. Rare and Extreme Wildland Fire in Sakha in 2021. *Atmosphere* **2021**, *12*, 1572. [[CrossRef](#)]
 31. Hayasaka, H. Fire Weather Conditions in Boreal and Polar Regions in 2002–2021. *Atmosphere* **2022**, *13*, 1117. [[CrossRef](#)]
 32. Hayasaka, H. Peatland Fire Weather Conditions in Sumatra, Indonesia. *Climate* **2023**, *11*, 92. [[CrossRef](#)]
 33. Hayasaka, H. Fire Weather Conditions in Plantation Areas in Northern Sumatra, Indonesia. *Atmosphere* **2023**, *14*, 1480. [[CrossRef](#)]
 34. Usup, A.; Hayasaka, H. Peatland Fire Weather Conditions in Central Kalimantan, Indonesia. *Fire* **2023**, *6*, 182. [[CrossRef](#)]
 35. Yulianti, N.; Hayasaka, H. Recent Active Fires in Indonesia’s Southern Papua Province Caused by El Niño Conditions. *Remote Sens.* **2023**, *15*, 2709. [[CrossRef](#)]
 36. Worldview. Available online: <https://worldview.earthdata.nasa.gov/> (accessed on 12 October 2023).
 37. Climate and Average Weather Year Round in Villahermosa, Weather Spark. Available online: <https://weatherspark.com/y/10690/Average-Weather-in-Villahermosa-Mexico-Year-Round> (accessed on 1 October 2023).
 38. Thermal Low. Available online: https://glossary.ametsoc.org/wiki/Thermal_low (accessed on 30 November 2023).
 39. Climate and Average Weather Year Round in Colima, Weather Spark. Available online: <https://weatherspark.com/y/3823/Average-Weather-in-Colima-Mexico-Year-Round> (accessed on 1 October 2023).
 40. Galván, L.; Magaña, V. Forest fires in Mexico: An approach to estimate fire probabilities. *Int. J. Wildland Fire* **2020**, *29*, 753–763. [[CrossRef](#)]
 41. Domínguez, R.M.; Trejo, D.A.R. Forest Fires in Mexico and Central América. In Proceedings of the Second International Symposium on Fire Economics, Planning, and Policy: A Global View, Albany, CA, USA, 19–22 April 2008.
 42. Alizadeh, M.R.; Abatzoglou, J.T.; Adamowski, J.; Rad, A.M.; AghaKouchak, A.; Pausata, F.S.R.; Sadegh, M. Elevation-dependent intensification of fire danger in the western United States. *Nat. Commun.* **2023**, *14*, 1773. [[CrossRef](#)] [[PubMed](#)]
 43. Kelsey, V.; Riley, S.; Minschwaner, K. Atmospheric precipitable water vapor and its correlation with clear-sky infrared temperature observations. *Atmospheric Meas. Technol.* **2022**, *15*, 1563–1576. [[CrossRef](#)]

Disclaimer/Publisher’s Note: The statements, opinions and data contained in all publications are solely those of the individual author(s) and contributor(s) and not of MDPI and/or the editor(s). MDPI and/or the editor(s) disclaim responsibility for any injury to people or property resulting from any ideas, methods, instructions or products referred to in the content.